Available online at www.sciencedirect.com
SCIENCE DIRECT®
European Journal of Mechanics B/Fluids 24 (2005) 502–521

Free surface flow under gravity and surface tension due to an applied pressure distribution II Bond number less than one-third ☆

Montri Maleewong [a], Roger Grimshaw [b,*], Jack Asavanant [a]

[a] *Department of Mathematics and AVIC Center, Faculty of Science, Chulalongkorn University, Bangkok, Thailand*
[b] *Department of Mathematical Sciences, Loughborough University, Loughborough LE11 3TU, UK*

Received 15 September 2004; received in revised form 17 December 2004; accepted 10 January 2005

Available online 5 March 2005

Abstract

We consider the steady free surface two-dimensional flow due to a localized applied pressure distribution under the effects of both gravity and surface tension in water of a constant depth, and in the presence of a uniform stream. The fluid is assumed to be inviscid and incompressible, and the flow is irrotational. The behaviour of the forced nonlinear waves is characterized by three parameters: the Froude number, F, the Bond number, $\tau < 1/3$, and the magnitude and sign of the pressure forcing term ϵ. The fully nonlinear wave problem is solved numerically by using a boundary integral method. For small amplitude waves and $F < F_m < 1$ where F_m is a certain critical value where the phase and group velocities for linearized waves coincide, linear theory gives a good prediction for the numerical solution of the nonlinear problem in the case of a bifurcation from the uniform flow. As F approaches F_m, nonlinearity needs to be included in the problem. In this case the forced nonlinear Schrödinger equation is found to be an appropriate model to describe bifurcations from an unforced envelope solitary wave. In general, it is found that for given values of $F < F_m$ and $\tau < 1/3$, there exist both elevation and depression waves.

Keywords: Depression wave; Elevation wave; Trapped bubble; NLS; Gravity-capillary

1. Introduction

Free surface flow due to an applied pressure distribution in the presence of a uniform stream has been a much-studied problem for more than a century, with applications to the forcing of water waves by atmospheric disturbances, or due to moving obstacles such as ships. For the two-dimensional flow of an inviscid and incompressible fluid, the key parameters describing the waves are the Froude number $F = U/(gH)^{1/2}$ and the Bond number $\tau = T/\rho g H^2$ where U is the velocity of the uniform stream, H is the undisturbed water depth, ρ is the water density and T is the coefficient of surface tension. To these we add ϵ representing the magnitude and sign of the applied pressure forcing term.

The earliest works (e.g. Rayleigh [1]) used the linearized theory obtained by neglecting nonlinear terms in the free surface boundary conditions. Importantly, the linearized theory reveals that in order to obtain localized solutions it is necessary that

☆ This research was financially supported by the Thailand Research Fund through the Royal Golden Jubilee PhD. Program (Grant No. PHD/0189/2542) to the first and last authors.
* Corresponding author.
E-mail address: R.H.J.Grimshaw@lboro.ac.uk (R. Grimshaw).

0997-7546/$ – see front matter
doi:10.1016/j.euromechflu.2005.01.003

$F < 1$ when $\tau > 1/3$, or that $F < F_m < 1$ when $\tau < 1/3$ where F_m is that critical value for which the phase and group velocities coincide at a finite non-zero wavenumber (a formal definition is given in Section 3). In this paper we confine attention to the gravity-dominated case when $\tau < 1/3$; the case $\tau > 1/3$ was considered in a companion paper (Maleewong, Asavanant and Grimshaw, 2004 [2], hereafter denoted as MAG1). The validity of the linearized theory then requires that not only should the forcing be sufficiently small ($\epsilon \ll 1$), but also that F be bounded away from F_m when $\tau < 1/3$ and from 1 when $\tau > 1/3$. When both of these criteria fail, a weakly nonlinear theory can be constructed which leads to a forced nonlinear Schrödinger equation (fNLS) when $\tau < 1/3$, in contrast to a forced Korteweg–de Vries equation when $\tau > 1/3$ (MAG1).

The analysis from these linear and weakly nonlinear theories reveal that the flow behaviour changes when the critical value $\tau = 1/3$ is passed. That is, for $\tau > 1/3$, the solutions take the form of classical solitary waves. For small amplitudes and very long wavelengths, the appropriate model from the weakly nonlinear theory is the forced Korteweg–de Vries equation, whose unforced solitary wave solution has the well-known "sech^2"-profile. The connection between these and the fully nonlinear results is discussed in MAG1. In contrast, when $\tau < 1/3$, the problem is more complicated than this previous case. Now small-amplitude solutions take the form of envelope solitary waves, that is, localized wave packets, and the relevant weakly nonlinear model is the fNLS equation (see Akylas [3,4] for the case of zero surface tension, $\tau = 0$).

Unforced wave packet structures have attracted much attention over the past three decades. Zakharov [5] showed that the two-dimensional evolution of water waves in deep water can be described by the nonlinear Schrödinger equation (NLS). Later Hasimoto and Ono [6] derived this equation to study the stability of two-dimensional gravity waves in water of finite depth. This was then generalized to three-dimensional waves by Davey and Stewartson [7]. Kawahara [8] included the effects of surface tension for two-dimensional water waves, while the generalization to the three-dimensional case was done by Djordjevic and Redekopp [9]. Recently, Părău and Dias [10] treated the steady two-dimensional problem of gravity-capillary waves using a dynamical systems approach. They obtained a normal form equivalent to the steady fNLS model. A stability analysis for these waves in water of infinite depth was investigated by Calvo and Akylas [11]. In this paper, we extend the NLS equation obtained by Kawahara [8] to the fNLS equation, and we will show that there is good agreement between the results from this fNLS model and our fully nonlinear results.

For the fully nonlinear problem, we solve the set of governing equations using an accurate numerical method. Vanden-Broeck and Dias [12] used a boundary integral equation method to solve the gravity-capillary wave due to pressure distribution in water of infinite depth. Then Dias, Menasce and Vanden-Broeck [13] utilized the same method to solve the unforced case for both infinite and finite depth. They found some new families of gravity-capillary waves.

In our work, we apply a similar boundary integral method to investigate elevation and depression waves for both forced and unforced cases. A localized symmetric surface pressure distribution with a finite span is applied on the free surface to generate gravity-capillary waves in water of finite depth. We take $\tau < 1/3$ and assume that the solution is symmetric, and the flow is subcritical. We find that both depression and elevation waves exist for $\epsilon \geqslant 0$ and $\epsilon < 0$. For some cases of depression waves, a limiting configuration with a trapped bubble is found. This type of solution was previously found by Hunter and Vanden-Broeck [14] in the unforced case.

In Section 2 we describe the formulation of the fully nonlinear problem. Some aspects from the linearized theory are discussed in Section 3. In Section 4 we provide the boundary integral method for the fully nonlinear problem. Our numerical results are presented in Section 5. Analysis of the weakly nonlinear theory associated with the fNLS equation, including a comparison with the numerical results is given in Section 6. We conclude with a discussion in Section 7.

2. Formulation

We consider a steady two-dimensional free-surface flow with a localized applied pressure distribution in water of constant depth. The fluid is assumed to be inviscid and incompressible, and the flow is irrotational. The fluid domain is bounded below by a rigid bottom and above by a free surface. We choose Cartesian coordinates with the x-axis along the bottom and the y-axis directed vertically upwards. Gravity is acting in the negative y-direction. Surface tension is included in the dynamic boundary condition on the free surface. Far upstream, the flow is assumed to be uniform with constant velocity U and constant depth H. The formulation and the corresponding linearized theory is described in MAG1 but for completeness we summarize it here.

The problem is made non-dimensional by choosing U, H and UH as velocity, length and velocity potential scales respectively. In terms of these dimensionless variables, the equations governing the motion written in terms of the velocity potential $\phi(x, y)$ are as follows.

$$\phi_{xx} + \phi_{yy} = 0, \quad -\infty < x < \infty, -1 < y < \eta(x), \tag{1}$$

$$\phi_y = 0, \quad y = -1, \tag{2}$$

$$\phi_y = \phi_x \eta_x, \quad y = \eta(x), \tag{3}$$

$$\frac{F^2}{2}(\phi_x^2+\phi_y^2-1)+\eta=\tau\frac{\eta_{xx}}{(1+\eta_x^2)^{3/2}}-\frac{F^2}{2}\epsilon p(x),\quad y=\eta(x). \tag{4}$$

Here η is the free surface elevation, F is the Froude number $U/\sqrt{gH}$, τ is the Bond number $T/\rho g H^2$ and $\epsilon p(x)$ is the pressure forcing term $2p_a(x)/\rho U^2$. For given values of F and τ, and the applied pressure $\epsilon p(x)$, the velocity potential $\phi(x, y)$ and the free surface elevation $\eta(x)$ are to be determined, subject to the boundary condition that $\phi \to x$ as $x \to \infty$. This completes the formulation.

Here we assume either that the forcing function has compact support, or that it decays rapidly at infinity. Further, we shall also assume that $p(x)$ is symmetric, monotone and non-negative ($p(x) = p(-x) \geqslant 0$ for all x, and $p_x(x) \leqslant 0$ for $x \geqslant 0$). A typical compact forcing function is

$$p(x)=\exp\left({x_b}^2/(x^2-{x_b}^2)\right)\quad \text{for } |x|\leqslant x_b,$$

while $p(x) = 0$ for $|x| > x_b$ and x_b is the span width of the forcing.

3. Linear theory

Before proceeding to numerical simulations of the fully nonlinear problem, it is instructive to consider the linearized theory. We put $\phi = x + \bar{\phi}(x, y)$, where $\bar{\phi}(x, y)$ is the small perturbation of ϕ. Substituting this into the governing equations (1)–(4) and linearizing around the uniform stream, we obtain the set of linear governing equations as follows (the bar symbol is omitted),

$$\phi_{xx}+\phi_{yy}=0,\quad -\infty<x<\infty,\ -1<y<0, \tag{5}$$

$$\phi_y=0,\quad y=-1, \tag{6}$$

$$\phi_y=\eta_x,\quad y=0, \tag{7}$$

$$F^2\phi_x+\eta=\tau\eta_{xx}-\frac{F^2}{2}\epsilon p(x),\quad y=0. \tag{8}$$

Next we define the Fourier transform of ϕ and its inverse transform as

$$\hat{\phi}=\int_{-\infty}^{\infty}\phi\,\mathrm{e}^{-ikx}\,\mathrm{d}x,\qquad \phi=\frac{1}{2\pi}\int_{-\infty}^{\infty}\hat{\phi}\,\mathrm{e}^{ikx}\,\mathrm{d}k$$

respectively, with an analogous definitions for η, $\hat{\eta}$, and the pressure forcing term. We apply this Fourier transform to the set of linear equations (5)–(8). After satisfying the bottom boundary condition (6), we find the solution of (5) for $\hat{\phi}$ is

$$\hat{\phi}=\frac{a(k)\cosh k(y+1)}{\cosh k}.$$

The remaining boundary conditions then yield the Fourier transform $\hat{\eta}$ of the free surface elevation as

$$\hat{\eta}=-\frac{F^2}{2}\frac{\epsilon\hat{p}}{[(1+\tau k^2)-F^2k\coth k]}. \tag{9}$$

First, we consider unforced waves. For these, the linear dispersion relation for periodic waves is readily obtained by setting $\epsilon = 0$, which from (9) can only be satisfied if its denominator is zero, that is,

$$F^2=(1+\tau k^2)\frac{\tanh k}{k}.$$

Now localized solutions to the linear forced problem, or indeed to the fully nonlinear forced problem, are only expected to exist for those values of F^2 such that there is no real wavenumber k for which this dispersion relation can be satisfied. It is then easily shown that this is achieved either for $\tau > 1/3$ with $0 < F^2 < 1$, or for $\tau < 1/3$ with $0 < F < F_m < 1$ where F_m is defined as the value of F at $k = k_m$ where $\mathrm{d}F/\mathrm{d}k = 0$. Then F_m, k_m are given parametrically as functions of $\tau(< 1/3)$ by

$$\begin{aligned}&\frac{1+\tau k_m^2}{1-\tau k_m^2}=\frac{\sinh 2k_m}{2k_m},\\ &F_m^2=(1+\tau k_m^2)\frac{\tanh k_m}{k_m}=(1-\tau k_m^2)\frac{\sinh^2 k_m}{k_m^2}.\end{aligned} \tag{10}$$

We are now interested in the possible solitary wave bifurcations occurred in the dispersion curve. It is well known that bifurcation phenomenon occurs when the wave speed c equals the group speed c_g or $\mathrm{d}F^2/\mathrm{d}k = 0$ (Grimshaw and Iooss [15]).

There are 3 possibilities: (i) $k = 0$, (ii) $k = k_m$ for k_m real and (iii) $k = k_c$ is a complex number.

(i) When $k = 0$, we have $F = 1$. This yields a long wave solution, namely the "solitary wave". This solitary wave solution bifurcates from the uniform stream at the critical Froude number $F = 1$. These monotonic types of solitary wave exist when $0 < F < 1$ and $\tau > 1/3$. In this case the Korteweg–de Vries equation is a good prediction to these types of waves for small amplitudes (Hunter and Vanden-Broeck [14]). Existence of these waves has been proved by Amick and Kirchgässner [16]. Numerical results with the connection to the forced Korteweg–de Vries equation for small amplitude waves can be found in the companion paper MAG1.

(ii) Here k_m, F_m are determined from (10). The solitary wave solutions in this case exhibit the form of an envelope wave when $\tau < 1/3$ and $F < F_m < 1$. They have damped oscillations in the tail of the waves. Weakly nonlinear analysis reveals that these equations are governed by the nonlinear Schrödinger equation (Akylas [4]). Moreover, the existence of these types of waves has been proved by Iooss and Kirchgässner [17]. In this paper, we adapt the unforced NLS derived by Kawahara [8] to investigate the behavior of modulated gravity-capillary waves in the neighborhood of F_m. A fNLS model is used to explained the nonlinear behavior of solutions due to the applied pressure distribution. The connection between the fNLS model and our fully nonlinear results is discussed in Section 6.

(iii) Another possible bifurcation occurs when $k = k_c = \mathrm{i}\sigma_c$ is a pure imaginary solution of (10), i.e.,

$$\frac{1 - \tau\sigma_c^2}{1 + \tau\sigma_c^2} = \frac{\sin 2\sigma_c}{2\sigma_c},$$

with the corresponding value of F_c obtained from the linear dispersion relation. This bifurcation represents the situation when a solitary wave of finite amplitude changes from a wave with monotonic decay at infinity to one with decaying oscillations at infinity. However, we did not investigate this situation in this present paper; for further details see Dias and Iooss [18].

Next we return to a consideration of the forced problem when ϵ is small. Here, we expect the forced solutions to bifurcate either from the uniform stream, or from the appropriate solitary wave solution. In the former case, the solution is given to leading order by (9), while in the latter case the leading order solution will be close to the relevant solitary wave, that is, either the KdV solitary wave if $\tau > 1/3$ or the solitary wave solution of the NLS model if $\tau < 1/3$.

Considering the linearized solution (9), let us define $f(k) = (1 + \tau k^2) - F^2 k \coth k$. It can be shown that $f(k)$ is always positive whenever F is chosen to ensure the existence of only localized solutions (that is, $0 < F < 1$ for $\tau > 1/3$, and $0 < F < F_m$ for $\tau < 1/3$). For a localized forcing function $p(x)$ which is symmetric, monotone and non-negative ($p(x) = p(-x) \geqslant 0$ for all x, and $p_x(x) \leqslant 0$ for $x \geqslant 0$) it can be shown that the Fourier transform $\hat{p}$ is real and positive for all k. Hence, from the definition of the Fourier transform of η, we can infer that η is symmetric and that $\eta(0) < 0 (> 0)$ according as $\epsilon > 0 (< 0)$.

4. Numerical method for the nonlinear problem

In this section we reformulate the problem as an integral equation for the unknown free surface variables. Let us introduce the complex potential function $f(z) = \phi(x, y) + \mathrm{i}\psi(x, y)$ where ϕ and ψ are the usual potential function and stream function respectively. We define the complex velocity w by $w = \mathrm{d}f/\mathrm{d}z = u - \mathrm{i}v$. Here u and v are velocity components in the x- and y-directions. On the free surface, we set the streamline to be $\psi = 0$. As a consequence, the bottom defines another streamline $\psi = -1$. Here we choose $\phi = 0$ at the intersection point between the free surface and the symmetry line of the forcing function. The flow domain in the complex f-plane is simply an infinite strip.

To obtain the required integral equation, we adapt the boundary integral technique used by Schwartz [19], Vanden-Broeck and Dias [12], Asavanant and Vanden-Broeck [20]. We map the flow domain in the complex f-plane onto the lower half of the complex ζ-plane by the transformation $\zeta = \alpha + \mathrm{i}\beta = \exp(\pi f)$. Instead of using $u(\phi, \psi)$ and $v(\phi, \psi)$, we define w as $w = u - \mathrm{i}v = \exp(\varphi - \mathrm{i}\theta)$. The hodograph variables φ and θ are real-valued functions of α and β. The kinematic boundary condition on the bottom ($\psi = -1$) implies that $\theta(\alpha, 0) = 0$ for $\alpha < 0$. Next we apply the Cauchy's integral formula to the function $\varphi - \mathrm{i}\theta$ in the ζ-plane with a contour consisting of the real axis and the circumference of a half circle of arbitrary large radius in the lower half plane. After taking the real part, we get

$$\varphi(\alpha) = \frac{1}{\pi} \int_0^\infty \frac{\theta(\alpha')}{\alpha' - \alpha}\,\mathrm{d}\alpha' \quad \text{on } \beta = 0. \tag{11}$$

Here $\varphi(\alpha) = \varphi(\alpha, 0)$ and $\theta(\alpha) = \theta(\alpha, 0)$. The dynamic boundary condition on the free surface can be written as

$$F^2\,\mathrm{e}^{2\varphi} + 2y + F^2\,\widetilde{P} - 2\tau\,\mathrm{e}^{\varphi}\,\frac{\partial\theta}{\partial\phi} = 2 + F^2 \tag{12}$$

where τ is the Bond number and $\widetilde{P}(\phi)$ is the forcing function to be defined later. Eqs. (11) and (12) define a system of nonlinear integral equations for the unknown function $\theta(\alpha)$ on the free surface $0 < \alpha < \infty$. Finally, the position of the free surface y can be evaluated by using the relation

$$y(\alpha) = 1 + \frac{1}{\pi}\int_0^{\alpha} \frac{\exp(-\varphi(\alpha_0))\sin\theta(\alpha_0)}{\alpha_0}\,\mathrm{d}\alpha_0. \tag{13}$$

To find numerical solutions of this nonlinear system, we use the change of variable $\alpha = \mathrm{e}^{\pi\phi}$. Eqs. (11) and (13) become

$$\varphi'(\phi) = \int_0^{\infty} \frac{\theta'(\phi_0)\exp(\pi\phi_0)}{\exp(\pi\phi_0) - \exp(\pi\phi)}\,\mathrm{d}\phi_0, \tag{14}$$

$$y'(\phi) = 1 + \int_0^{\phi} \exp\bigl(-\varphi'(\phi_0)\bigr)\sin\theta'(\phi_0)\,\mathrm{d}\phi_0. \tag{15}$$

Next we introduce equally spaced points in the potential function by $\phi_I = (I-1)E$, $I = 1, \ldots, N$. Here E is the mesh size. We evaluate the values of φ' in (14) at the midpoints $\phi_{I-1/2}$, $I = 1, \ldots, N$, by using the trapezoidal rule with summation over the points ϕ_I. The Cauchy principal value integrals can be evaluated as if they were ordinary integrals by using the symmetry of the quadrature and of the distribution of mesh points. We satisfy the dynamic boundary condition (12) at the midpoints. This yields $N-1$ nonlinear algebraic equations for the N unknowns θ_I. The last equation is obtained by imposing the condition $\theta_N = 0$. This system of nonlinear algebraic equations for N unknown θ_I is then solved by Newton's method.

We specify the pressure forcing on the free surface as

$$\widetilde{P} = \begin{cases} \epsilon \exp\left(\frac{1}{(\phi/\phi_B)^2 - 1}\right), & \text{if } |\phi| \leqslant |\phi_B|; \\ 0, & \text{otherwise.} \end{cases}$$

Note that it is convenient here to specify the pressure forcing in terms of ϕ rather than in terms of x. Thus, except in the linearized limit, the pressure forcing specified here differs from that specified at the end of Section 2. Of course, once the numerical solution has been obtained, it is straightforward to calculate the form of the pressure forcing as a function of x. For instance, the span length $2x_b$ of the pressure forcing is defined by the integration of $\exp(-\varphi)\cos\theta$ over ϕ from $-\phi_B$ to ϕ_B. For small amplitude solutions it is clear that $x_B \approx \phi_B$; from our numerical results we find that in general x_B increases with ϵ for elevation waves, but decreases with ϵ for depression waves. In the simulations reported here, we fix $\phi_B = 1.45$.

In the numerical procedure, the integral equation (14) must be truncated. Numerical accuracy is tested by varying the number of mesh points N and mesh spacing E. There are no variations in the numerical solutions when we choose $N \geqslant 401$ and $E \leqslant 0.05$. More details are given in MAG1. For the results reported for $\tau < 1/3$, we choose $N = 699$ and $E = 0.05$ for the case of elevation waves and use $N = 401$ and $E = 0.05$ for the case of depression waves. The reason why we use a larger value of N to compute the elevation waves is that the behavior of the elevation waves is more complicated than that of depression waves in the neighborhood of F_m. These numerical results will be shown and discussed in the next section.

5. Numerical results when $\tau < 1/3$

Here we restrict our attention to the case of symmetric subcritical flows ($F < F_m < 1$) when $\tau < 1/3$. The case of $\tau > 1/3$ was considered in our companion paper MAG1. In this section, we present our numerical results when $\tau = 0.25$ for depression and elevation waves (that is, according as $y(0) < 0$ or $y(0) > 0$ respectively). Note that for $\tau = 0.25$, $F_m = 0.9707$ (see (10)). The case of unforced solutions $\epsilon = 0$ will be referred to as depression solitary waves or elevation solitary waves.

5.1. Depression waves

It is found that solutions in the form of depression waves can be found for both ϵ positive and negative. The relationship between $F < F_m$ and $y(0)$ for various values of ϵ is shown in Fig. 1. For each branch of $\epsilon > 0$, there exist critical Froude numbers F_1 and F_2, both dependent on ϵ, such that there is a unique solution when $0 < F < F_1$, two solutions when $F_1 < F < F_2$, and no solutions when $F_2 < F < 1$. One family of solutions can be viewed as a perturbation from a uniform stream and the other is a perturbation from a depression solitary wave. Similar solution behaviours but with different wave profiles can also be found in the case of $\tau > 1/3$ (see MAG1). The major difference is that there are more inflexion points on the wave

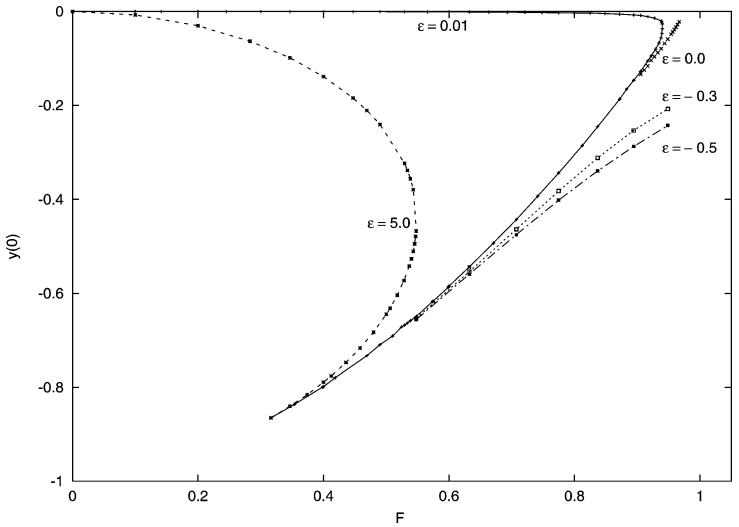

Fig. 1. Relationship between F and $y(0)$ when $\tau = 0.25$ for various values of ϵ.

profiles in the present case of $\tau < 1/3$, indicating that these waves resemble wave packets when the amplitude is small. Some typical free surface profiles are shown in Fig. 2. Fig. 2 (a) and (b) show the nonuniqueness of solutions for the same value of F. As the critical value of F_1 is reached, the solutions approaches its limiting configuration with a trapped bubble as shown in Fig. 2(c). This type of solutions in the case of unforced wave was previously found by Hunter and Vanden-Broeck [14], and Longuet-Higgins [21].

For $\epsilon = 0$, a branch of depression solitary waves exists in the range $F_1 < F < F_m$. As F approaches F_m, there are more inflexion points on the free surface and the wave profile takes the form of an envelope solitary wave (that is, a wave packet). The weakly nonlinear model associated with the NLS equation reveals the existence of these solutions (Akylas [4]). We will defer the comparisons between our nonlinear and the weakly nonlinear model to Section 6. Due to the occurrence of inflexion points on the free surface when F is close to F_m, the computation requires more mesh points in order to get the desired solution accuracy. Thus, computing solutions in the limit $F \to F_m$ becomes increasingly difficult.

When $\epsilon < 0$, there exists a unique solution of depression waves that bifurcate from $\epsilon = 0$ for $F_1 < F < F_m$ as shown in Fig. 1. The limiting configuration with a trapped bubble occurs when $F \to F_1$. As F increases, the depression wave develops more inflexion points whereas the wavelength increases. The calculations again become formidable as F approaches F_m. Typical free surface profiles for $\epsilon = -0.5$ and $F = 0.7071$ and 0.8945 are shown in Fig. 2 (d) and (e) respectively.

5.2. Elevation waves

Similarly for the case of depression waves, there are elevation wave solutions for both ϵ positive and negative. The relationship between F and $y(0)$ for various values of $\epsilon < 0$ is shown in Fig. 3. The blow up of the turning point of the $\epsilon = 0$ and -0.01 branches is shown in Fig. 4. Similar behaviour is also found in the case of very small $\epsilon > 0$ which we will discuss further in Section 6. For larger negative forcing ($\epsilon = -0.5$), the turning point on the solution curve becomes very sharp. The portions of the solution curve before and after the turning point almost coincide despite the difference in the profiles.

For the $\epsilon < 0$ branch, there exist critical Froude numbers F_3 and F_4, again dependent on ϵ, such that there is a unique solution when $0 < F < F_3$, two solutions when $F_3 < F < F_4$, and no solutions when $F_4 < F < F_m$. One family of solutions can be viewed as a perturbation from a uniform stream and the other is a perturbation from a solitary wave. These results differ from the case of $\tau > 1/3$ in that only the perturbation solution from uniform stream can be found for $0 < F \leqslant 1$.

The development of wave profiles along the branch of $\epsilon = -0.01$ is depicted in Fig. 5(a)–(c). Fig. 5 (a) and (b) refer to solutions along the lower portion of the curve before the turning point $F = F_4$, whereas Fig. 5(c) corresponds to solution along the upper portion of the curve at the critical value $F = F_3$.

The branch of an elevation solitary wave ($\epsilon = 0$) is also found and shown in Fig. 4. It should be noted that these solutions bifurcate from the critical value F_m. A typical free surface profile of envelope solitary wave is shown in Fig. 5(d). The connection to the weakly nonlinear theory of these solutions is discussed in the next section.

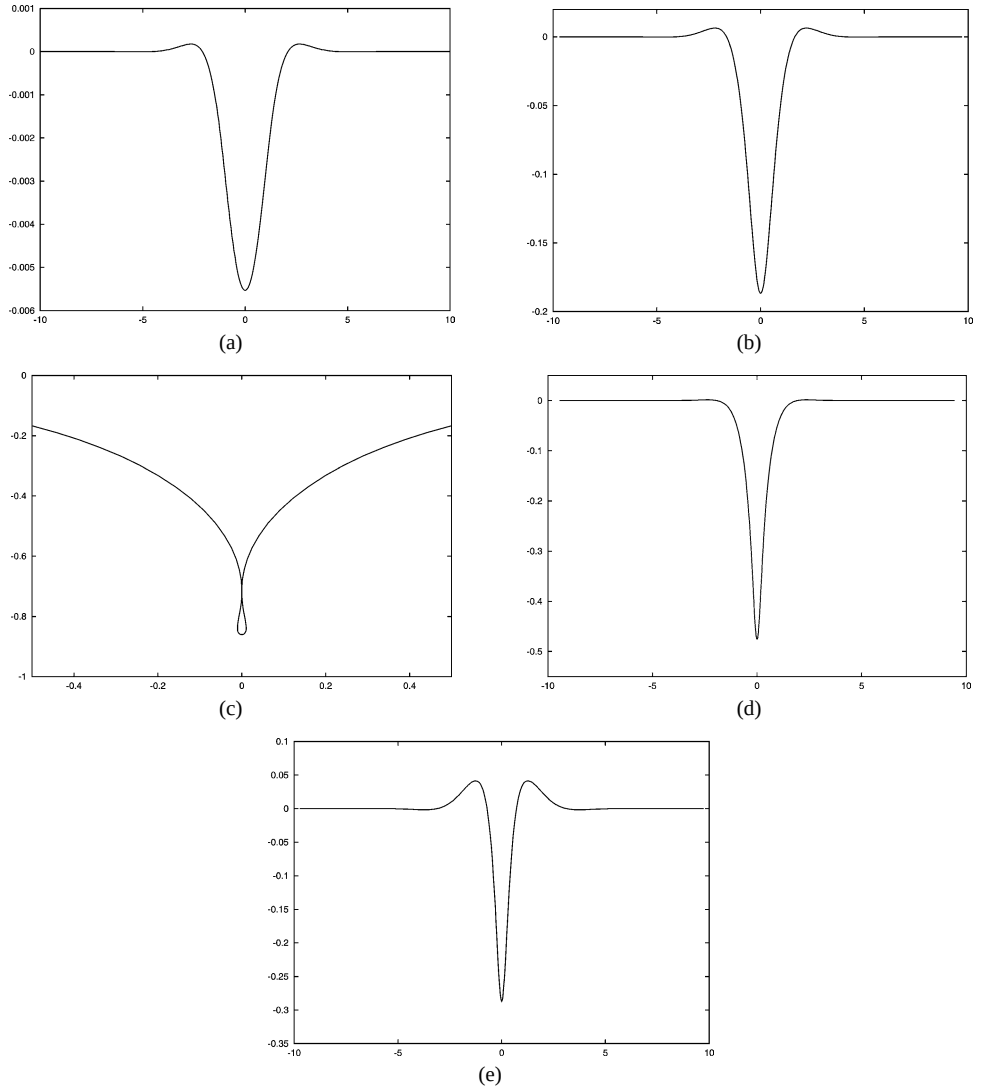

Fig. 2. Typical free surface profiles of depression waves when $\tau = 0.25$. (a) $F = 0.8717$, $\epsilon = 0.01$; (b) $F = 0.8717$, $\epsilon = 0.01$; (c) $F = 0.3245$, $\epsilon = 0.01$; (d) $F = 0.7071$, $\epsilon = -0.5$; (e) $F = 0.8945$, $\epsilon = -0.5$.

Recently, a numerical study of gravity-capillary solitary waves in water of finite depth was reported by Dias, Menasce and Vanden-Broeck [13]. It is interesting to compare our results shown in Fig. 4. to theirs. To do this, we define the dimensionless parameter

$$\alpha = \frac{\tau}{F^4}.$$

The branch of elevation solitary wave is replotted to show the relationship between α and $y(0)$. To vary α, we fix $\tau = 0.25$ and vary F, $0.866 < F < 0.975$. Then α is varied, $0.444 > \alpha > 0.277$. The relationship between α and $y(0)$ for fixed τ is shown in Fig. 6(a). Similarly, we can vary α by fixing $F = 0.9486$. This is equivalent to using τ in the range $(0.224, 0.333)$ which corresponds to $\alpha \in (0.276, 0.412)$. The relationship between α and $y(0)$ for a given value of F is shown in Fig. 6(b). The development of free surface profiles on the curve of Fig. 6(b) is shown in Fig. 7(a)–(c). As α decreases, more inflexion points in the wave profile become apparent. We are unable to find solutions for $\alpha < 0.276$. In addition, the wave amplitude approaches zero as α increases. The relationship between $y(0)$ and $y''(0)$ corresponding to the wave profiles Fig. 7(a)–(c) is shown in Fig. 7(d). It should be noted that Dias, Menasce and Vanden-Broeck defined $T/\rho U^2$ as a unit length. Therefore the scaling factor of the length scale as compared to ours differ by $F^2\alpha$. After adjusting this scaling factor we find that the curve

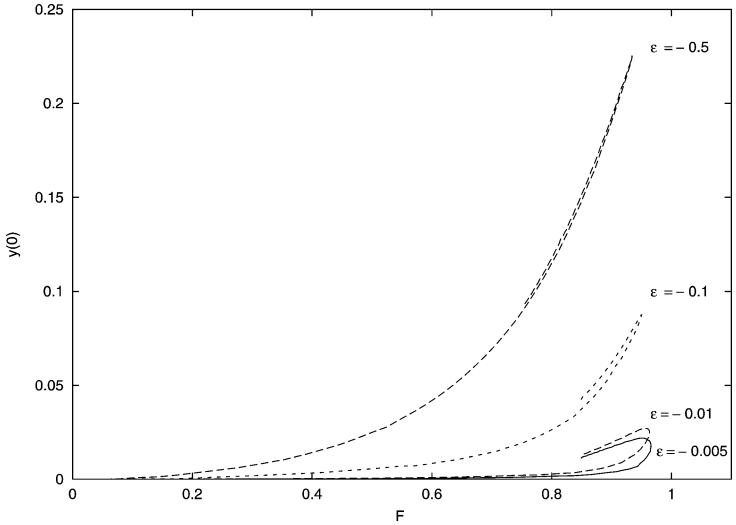

Fig. 3. Relationship between F and $y(0)$ when $\tau = 0.25$ for various values of $\epsilon < 0$. Note that the solution curves for positive forcing $\epsilon > 0$ are shown in Fig. 14(c).

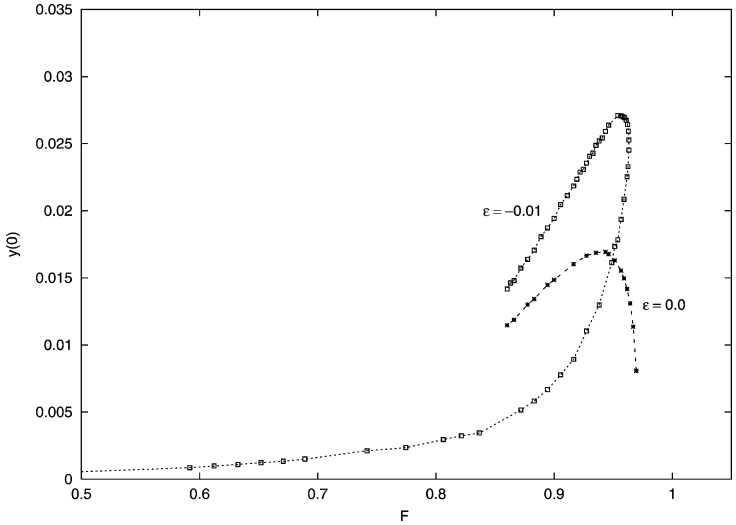

Fig. 4. Blow up of the solution branches for $\epsilon = 0$ and -0.01.

in Fig. 6(b) of our work is in good agreement with theirs (Ref. Fig. 4.1). This constitutes an accuracy check of our numerical computations.

Moreover, we also find a new family of solutions when $\tau = 0.25$ and $\epsilon = 0$. The wave profile is in the form of a two-humped solution (Fig. 8(a)). As F increases, the wave profile (Fig. 8(b)) develops more inflexion points. When F decreases, the distance between the undisturbed level and the humps increases (Fig. 8(c)).

Next, to understand the effects of a pressure distribution on these two-hump solutions, we vary $\epsilon > 0$ and < 0. The wave profiles for increasing $\epsilon > 0$ are shown in Fig. 9 (a) and (b). The behavior at the origin changes rapidly as ϵ varies and the wave profile develops more humps as ϵ increases. It should be noted that these multi-hump solutions apparently exist only for a small range of Froude number, and that $y(0) < 0$. Due to the complexity in their solution structure, we do not show this solution branch in Fig. 3. Next we observe from Fig. 10 (a) and (b) that in order to get relatively similar wave amplitudes $y(0)$ for the case when $\epsilon < 0$ it is necessary to increase considerably the magnitude of ϵ. This shows the dominant role of surface tension in the dynamic boundary condition.

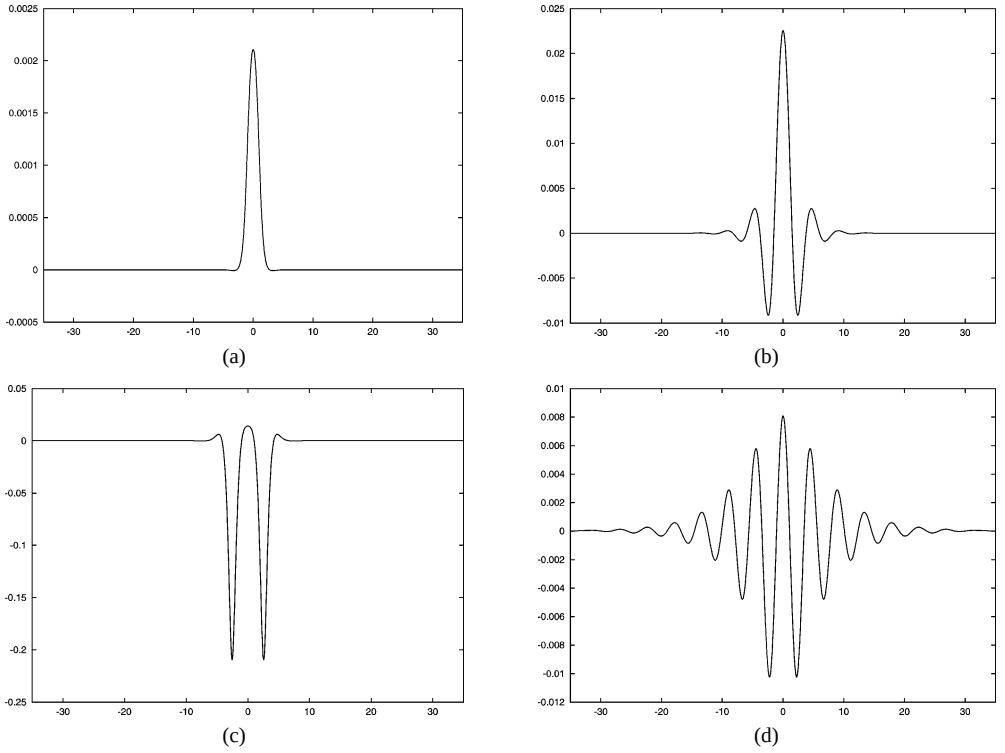

Fig. 5. Typical free surface profiles of elevation waves when $\tau = 0.25$. (a) $F = 0.7416$, $\epsilon = -0.01$; (b) $F = 0.9618$, $\epsilon = -0.01$; (c) $F = 0.8602$, $\epsilon = -0.01$; (d) $F = 0.9695$, $\epsilon = 0.0$.

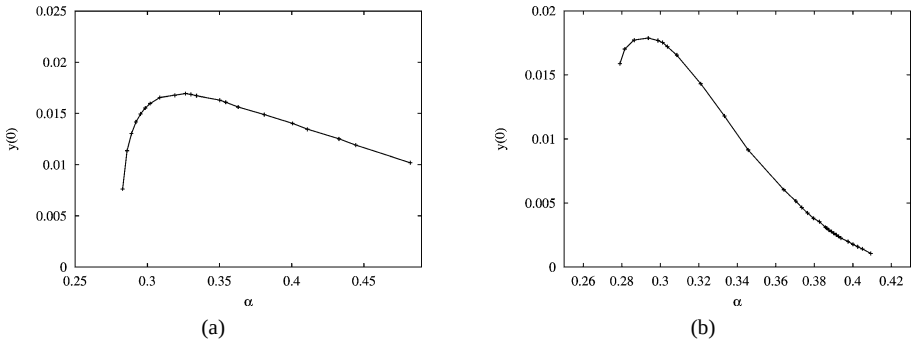

Fig. 6. $(\alpha, y(0))$-plane. (a) $(\alpha, y(0))$-plane, $\epsilon = 0.0$, varied F; (b) $(\alpha, y(0))$-plane, $\epsilon = 0.0$, varied τ.

6. Weakly nonlinear theory

6.1. Nonlinear Schrödinger Equation (NLS)

In this section, the weakly nonlinear theory for modulated gravity-capillary waves in water of finite depth is considered. First we consider unforced waves. Initially in this section we use the original dimensional coordinates for unsteady waves in standard notation in order that we can most easily make comparison with earlier works. In a frame of reference moving with the group velocity, $c_g = \partial\omega/\partial k$, we can write the solution for the free surface elevation η as

$$\eta = \mu A \exp \mathrm{i}(kx - \omega t) + c.c. + \cdots. \tag{16}$$

Here A is the amplitude of a wave packet with oscillation wavenumber k and frequency ω satisfying the linear dispersion relation. We introduce $\xi = \mu(x - c_g t)$ and $T = \mu^2 t$ and let $A = A(\xi, T)$, and $\mu \ll 1$. Then the envelope A is governed by the

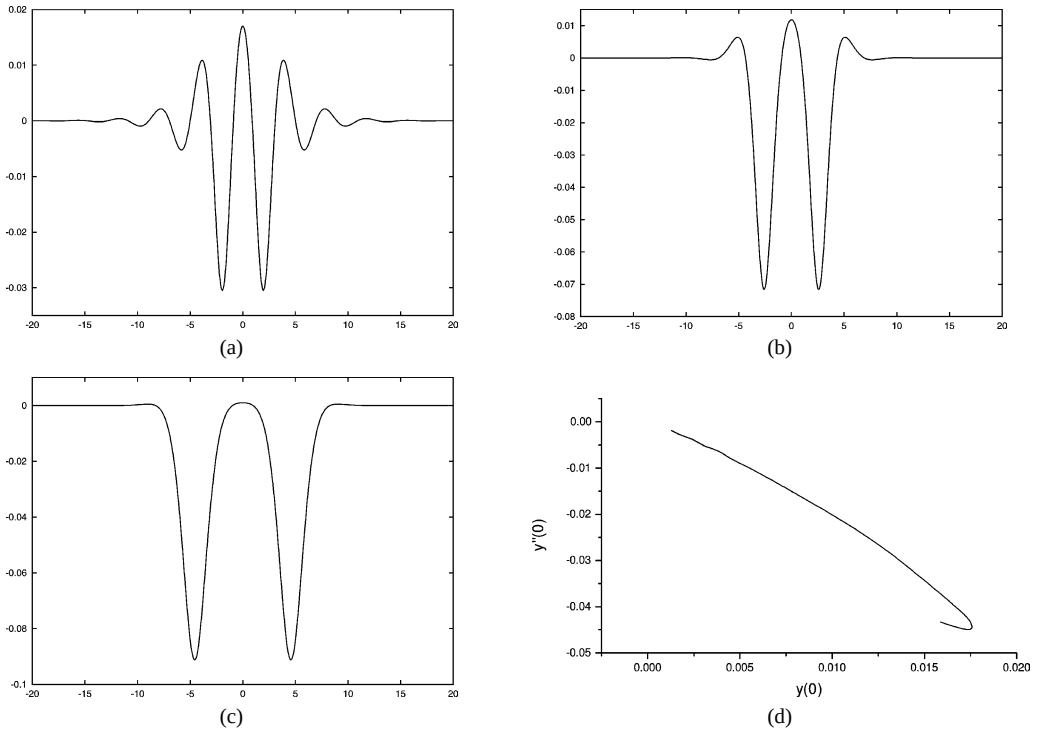

Fig. 7. (a)–(c) Typical free surface profiles of elevation waves when $F = 0.9486$ and $\epsilon = 0.0$. (a) $\tau = 0.228$, $\alpha = 0.281$; (b) $\tau = 0.270$, $\alpha = 0.331$; (c) $\tau = 0.333$, $\alpha = 0.412$; (d) $(y(0), y''(0))$-plane.

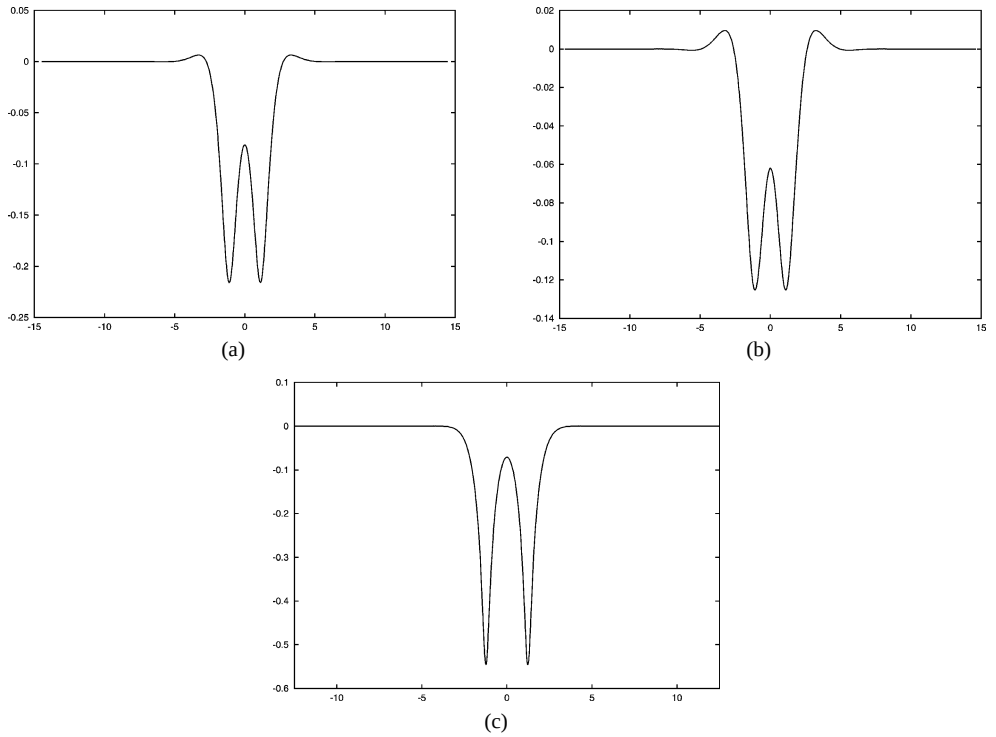

Fig. 8. Typical free surface profiles when $\tau = 0.25$ and $\epsilon = 0.0$. (a) $F = 0.8602$; (b) $F = 0.9165$; (c) $F = 0.6323$.

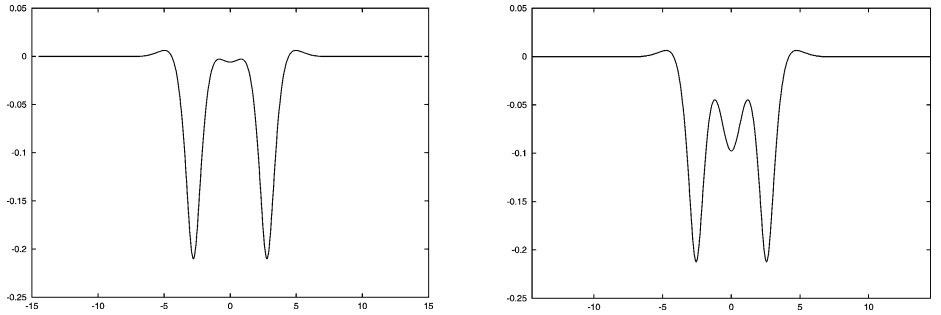

(a) (b)

Fig. 9. Typical free surface profiles when $\tau = 0.25$ and $F = 0.8602$, $\epsilon > 0$. (a) $\epsilon = 0.03$; (b) $\epsilon = 0.15$.

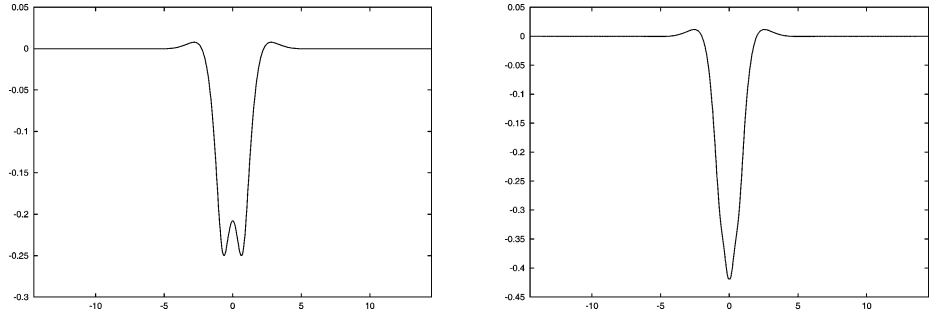

(a) (b)

Fig. 10. Typical free surface profiles when $\tau = 0.25$ and $F = 0.8602$, $\epsilon < 0$. (a) $\epsilon = -0.3$; (b) $\epsilon = -2.5$.

NLS equation (see Kawahara [8] for the derivation)

$$\mathrm{i}A_T + \lambda A_{\xi\xi} + \nu|A|^2 A = 0 \tag{18}$$

where

$$\lambda = \frac{1}{2}\frac{\mathrm{d}^2\omega}{\mathrm{d}k^2} = -\frac{1}{8\omega^3}\big\{(g^2 - 6gTk^2 - 3T^2k^4)\sigma^2 - 2(g + Tk^2)(g + 3Tk^2)kh(\sigma - \sigma^3) + (g + Tk^2)^2k^2h^2(1 + 2\sigma^2 - 3\sigma^4)\big\} \tag{19}$$

and

$$\nu = -\frac{k^2}{4\omega\sigma}\left[\frac{k}{\{g\sigma^2 + Tk^2(\sigma^2 - 3)\}}\big\{g^2(9\sigma^4 - 10\sigma^2 + 9) + gTk^2(15\sigma^4 - 44\sigma^2 + 30) + T^2k^4(6\sigma^4 - 25\sigma^2 + 21)\big\} + \frac{2(g + Tk^2)}{(\mathrm{d}\omega/\mathrm{d}k)^2 - gh}\big\{6(g + Tk^2)\sigma - 2(g + 3Tk^2)\sigma^3 + 3(g + Tk^2)kh(1 - \sigma^2)^2\big\}\right] \tag{20}$$

where $\sigma = \tanh kh$,

$$\omega^2 = gk(1 + \tau k^2h^2)\tanh kh.$$

We seek a solution of (18) in the form of an envelope solitary wave, that is,

$$A(\xi, T) = R(\chi)\exp \mathrm{i}(\kappa\xi - \sigma T) \tag{21}$$

where $\chi = \xi - VT$ is a moving frame with respect to the frame (ξ, T), and V and κ are constants. Substituting Eq. (21) in the NLS equation (18) leads to an ordinary differential equation for $R(\xi)$,

$$\lambda\frac{\mathrm{d}^2R}{\mathrm{d}\chi^2} + (\sigma - \lambda\kappa^2)R + \nu R^3 = 0 \quad \text{with } V = 2\kappa\lambda. \tag{22}$$

Imposing the condition that $R(\chi)$ and $\mathrm{d}R(\chi)/\mathrm{d}\chi \to 0$ for $\chi \to \pm\infty$, the following result is obtained

$$R = a\,\mathrm{sech}\,\gamma\xi, \quad \text{with } \gamma^2 = \frac{\nu a^2}{2\lambda},\ \sigma = \lambda(\kappa^2 - \gamma^2). \tag{23}$$

Here κ and the amplitude a are two free parameters. Note that this solution is valid only under the condition that $\nu\lambda > 0$.

Next, we consider the higher-order NLS equation given by

$$\mathrm{i}A_T + \lambda A_{\xi\xi} + \nu|A|^2A + \mathrm{i}\mu\{\lambda_1 A_{\xi\xi\xi} + \nu_1|A|^2A_\xi + \nu_2 A^2A_\xi^*\} = 0. \tag{24}$$

Here

$$\lambda_1 = -\frac{1}{6}\frac{\partial^3\omega}{\partial k^3}$$

while the higher-order nonlinear coefficients ν_1, ν_2 can be expressed as derivatives with respect to k of the nonlinear coefficient ν, but it will turn out that their exact values are not needed here. An envelope solitary wave is now given by

$$A = \big\{R(\chi) + \mathrm{i}\mu R_1(\chi)\big\}\exp\mathrm{i}(\kappa\xi - \sigma T). \tag{25}$$

Without any loss of generality we can assume that both R, R_1 are real-valued, as any imaginary part to R_1 can be absorbed into R. Substitution into Eq. (24) now yields

$$(\lambda - 3\mu\lambda_1\kappa)R_{\chi\chi} + (\sigma - \lambda\kappa^2 + \mu\lambda_1\kappa^3)R + \big(\nu - \mu(\nu_1 - \nu_2)\kappa\big)R^3 + \mu(V - 2\kappa\lambda)R_{1\chi} = 0, \tag{26}$$

$$\mu\big\{\lambda_1 R_{1\chi\chi} + (\sigma - \lambda\kappa^2)R_1 + \nu R^2R_1\big\} + \mu F_1 = 0 \tag{27}$$

where

$$F_1 = \lambda_1 R_{\chi\chi\chi} - (V_1 + 3\lambda_1\kappa^2)R_\chi + (\nu_1 + \nu_2)R^2R_\chi. \tag{28}$$

Here we have expanded $V = 2\kappa\lambda + \mu V_1$. At leading order in μ, we obtain the previous result that R, V are given by (22) and (23). Next, we see that Eq. (26) for R is identical in form to Eq. (22) and so has the same solution (23) with modified coefficients. Next Eq. (27) for R_1 reduces to

$$\big\{\lambda R_{1\chi\chi} + (\sigma - \lambda\kappa^2)R_1 + \nu R^2R_1\big\} + F_1 = 0. \tag{29}$$

This inhomogeneous equation for R_1 needs a compatibility condition, that is F_1 should be orthogonal to R which is the bounded solution of the homogeneous equation for R_1 (that is, (27) with $F_1 = 0$). Thus we require that

$$\int_{-\infty}^{\infty} RF_1\,\mathrm{d}\chi = 0. \tag{30}$$

But from (28), this is automatically satisfied and imposes no constraint on R_1. But if we look further into Eq. (27), we see that as $\chi \to \pm\infty$ F_1 has a leading order term proportional to $\exp(\mp\gamma\chi)$. Since the bounded solution to the homogeneous equation for R_1 is just R it will have the same behaviour. Hence the inhomogeneous equation will have solutions behaving like $\chi\exp(\mp\gamma\chi)$ as $\chi \to \pm\infty$, which is unacceptable. To avoid this we must put to zero the coefficient of $\exp(\mp\gamma\chi)$ in F_1 as $\chi \to \pm\infty$, which gives

$$V_1 = -3\lambda_1\kappa^2 \quad \text{so that} \quad V = 2\kappa\lambda_1 - \mu 3\lambda_1\kappa^2. \tag{31}$$

It now follows from (16) and (25) that the crests within the packet (16) move with the phase speed

$$c = \frac{\omega(k) + \mu\kappa c_g(k) + \mu^2\sigma}{k + \mu\kappa}, \tag{32}$$

$$\text{or} \quad c = \frac{\omega(k + \mu\kappa)}{k + \mu\kappa} - \frac{\mu^2\nu a^2}{2k} + \mathrm{O}(\mu^3). \tag{33}$$

That is the linear phase speed $c_p(k + \mu\kappa)$ slightly modified by finite amplitude effects. The envelope speed is

$$c_g(k) + \mu V = c_g(k + \mu\kappa) + \mathrm{O}(\mu^3) \tag{34}$$

after using (31) which is just the linear group velocity to leading order. Since these are not equal in general, the envelope solution defined by (16) is not a true solitary wave of the full equations.

But now, following the argument of Akylas [4] for the case $\tau = 0$, suppose that the linear phase speed has a local extremum at a particular value of the oscillation wave number $k = k_m$. Then the linear group velocity $c_g(k_m)$ is equal to the linear phase speed $c_p(k_m)$. It follows that the bifurcation condition for a small-amplitude envelope solitary wave can be found by equating (33) with (34) upon putting $k + \mu\kappa = k_m + \mu^2\Delta$ (that is, in effect $k = k_m$ and $\kappa = \mu\Delta$). This gives

$$\Delta = -\frac{\nu}{\lambda}\frac{a^2}{4k_m}. \tag{35}$$

Since here we can show that $\lambda(k = k_m) > 0$, and $\nu(k = k_m) > 0$ for gravity-capillary wave problem, we satisfy the condition that $\lambda\nu > 0$. Also then $\Delta < 0$ (that is, $k < k_m$) and so $c < c_p(k_m)$ as required.

6.2. Forced NLS equation (fNLS)

The derivation now follows the same path as above for the unforced NLS, but with a small extra forcing term (see Akylas [3] for the case when there is no surface tension, and Părău and Dias [10] for a different approach using normal form theory in the present case). To find the appropriate forcing term, it is sufficient to consider just the linear problem, which is,

$$\eta_t + U\eta_x = \phi_y, \quad \phi_t + U\phi_x + g(\eta - \tau h^2\eta_{xx}) = -\epsilon p(x) \quad \text{at } y = 0, \tag{36}$$

together with Laplaces equation for ϕ in $-h < y < 0$ and $\phi_y = 0$ at $y = -h$. This is just the unsteady version of the linearized problem for perturbations to a uniform stream discussed in Section 3, now in dimensional form. Next, as in Section 3, the Fourier transform in x of η is

$$\eta' = \int_{-\infty}^{\infty} \eta \exp(-\mathrm{i}kx)\,\mathrm{d}x, \tag{37}$$

which gives

$$\left\{\frac{\partial}{\partial t} + \mathrm{i}Uk\right\}^2 \eta' + \omega^2(k)\eta' = -k\tanh kh\epsilon p'. \tag{38}$$

This is easily solved, but here we are concerned only with the case when $U = U_m + \mu^2\delta$ where $U_m = c_m = \omega(k_m)/k_m$ being the minimum phase speed and occurs for a wavenumber k_m as before. Hence we look for a solution in which

$$\eta = \mu A(X, T)\exp(\mathrm{i}k_m x), \tag{39}$$

where $X = \mu x$, $T = \mu^2 t$. Note that for a truly steady solution, A would not depend on T but it is useful to retain this for now. Then, using (37) we get

$$\eta' = A'(\kappa, T) = \int_{-\infty}^{\infty} A(X, T)\exp(-\mathrm{i}\kappa X)\,\mathrm{d}X, \tag{40}$$

where $k - k_m = \mu\kappa$. Substitution into (38) then gives at leading order

$$\mathrm{i}A'_T - k_m\delta A' + \lambda\kappa^2 A' = -\frac{\epsilon\omega_m}{2g^*\mu^2}p', \tag{41}$$

where $g^* = g(1 + \tau h^2 k_m^2)$ and λ is given by (19) evaluated at $k = k_m$. Then, inverting the Fourier transform (40) we get

$$-\mathrm{i}A_T + k_m\delta A + \lambda A_{XX} = \frac{\epsilon\omega_m}{2g^*\mu^3}p\exp(-\mathrm{i}k_m x). \tag{42}$$

But here $p = p(X/\mu)$ and in the limit $\mu \to 0$ this is replaced by the δ-function, $\mu p_m\delta(X)$ where

$$p_m = \int_{-\infty}^{\infty} p(x)\exp(-\mathrm{i}k_m x)\,\mathrm{d}x$$

is the Fourier transform of $p(x)$ at $k = k_m$. Clearly we must choose $\epsilon = \mu^2$. So now we have

$$-\mathrm{i}A_T + k_m\delta A + \lambda A_{XX} = \frac{\omega_m p_m}{2g^*}\delta(X). \tag{43}$$

The right-hand side provides the connection between the pressure forcing in the full problem, and the forcing term in the forced NLS equation. In practice, as discussed below, we replace the δ-function with a smooth localized function whose area is unity. Finally we include the nonlinear term

$$-\mathrm{i}A_T + k_m\delta A + \lambda A_{XX} + \nu|A|^2 A = \frac{\omega_m p_m}{2g^*}\delta(X), \tag{44}$$

where ν is the same as in the unforced equation (18) but evaluated at $k = k_m$. Note the sign difference in the term A_T compared to (18) which is due to the different reference frame here.

We now seek a solution of (44) in the form of a steady envelope solitary wave, that is, $A = A(X)$ where we may take A as real-valued since when the forcing function is symmetric in X, then the Fourier transform p_m is real-valued. At the same time the equation is written in terms of the original unscaled variables. Thus (39) is replaced by

$$\eta = A(x)\exp(\mathrm{i}k_m x) + c.c., \tag{45}$$

and

$$\Delta k_m A + \lambda A_{xx} + \nu|A|^2 A = \frac{\omega_m \epsilon p_m}{2g^*}\delta(x) \tag{46}$$

where $\Delta = U - U_m$. This is an ordinary differential equation in $A(x)$, whose symmetric solutions for $x > (<)0$ are

$$A = a\,\mathrm{sech}\,\gamma(x \mp x_0), \quad \text{with } \gamma^2 = \frac{\nu a^2}{2\lambda},\ k_m\Delta = -\lambda\gamma^2. \tag{47}$$

Next we must use the jump condition at $x = 0$, obtained by integrating (46) across a small interval about the origin,

$$\lambda[A_x]_{0-}^{0+} = \frac{\omega_m \epsilon p_m}{2g^*}. \tag{48}$$

Hence we get

$$2\lambda\gamma a\,\mathrm{sech}\,\gamma x_0 \tanh\gamma x_0 = \frac{\omega_m \epsilon p_m}{2g^*}. \tag{49}$$

This determines x_0 in terms of p_m and a and so completes the solution. The Froude number is $F = U/\sqrt{gh}$ and so for a given F, we have Δ, hence a, γ from (47) and finally x_0 from (49). Note that the central amplitude is $a_m = a\,\mathrm{sech}\,\gamma x_0$. To obtain the bifurcation curve, we rewrite (49) as

$$\left\{\frac{\omega_m \epsilon p_m}{2g^*}\right\}^2 = -4\lambda a_m^2\left\{k_m\Delta + \frac{\nu a_m^2}{2}\right\}. \tag{50}$$

Thus the bifurcation curve is the same for $\epsilon > 0$ or < 0 and $a_m > 0$ or < 0. That is, the branch contains four solutions; one pair ($\epsilon > 0$) has a monotonic profile in $x > 0$ if $a_m < 0$ but is dimpled if $a_m > 0$, while the other pair ($\epsilon < 0$) has a monotonic profile in $x > 0$ if $a_m > 0$ but is dimpled if $a_m < 0$. But note that as in the forced Korteweg–de Vries model discussed in MAG1 for $\tau > 1/3$ case, not all branches are found. Here we must have $0 < \nu a_m^2/2 < -k_m\Delta$ (see (47)) and so the branches which lie outside the unforced solitary wave branch (that is, the case $\epsilon = 0$ so that $\nu a_m^2/2 = -k_m\Delta$) are not present. Also, there is no counterpart here of the "singular" solution of the forced Korteweg–de Vries model which remedied the corresponding defect there.

To find any missing branches the δ-function forcing must be replaced with a smooth forcing term. Suppose them, for instance, that we replace the δ-function in (46) with

$$K\,\mathrm{sech}(\gamma x), \tag{51}$$

where K is chosen to make the integral of (51) equal to unity. In this case we seek a solution of the form

$$A = a\,\mathrm{sech}(\gamma x), \tag{52}$$

but now we find that

$$\gamma^2 = \frac{\nu a^2}{2\lambda}, \quad \text{and} \quad a\left\{k_m\Delta + \frac{\nu a^2}{2}\right\} = \frac{K\omega_m \epsilon p_m}{2g^*}. \tag{53}$$

Note that now $a > 0$ (< 0) and $\epsilon p_m > 0$ (< 0) gives $k_m\Delta + \nu a^2/2 > 0$. Thus the "missing" branches are found. Conversely, the previous branches with $k_m\Delta + \nu a^2/2 < 0$ now require that $a > 0$ (< 0) as $\epsilon p_m < 0$ (> 0) and so the previous "dimpled" solutions are not found here. If they do exist for the fNLS equation with the forcing term (51) numerical integration is needed, but see below in Subsection 6.3 for more comment on this issue. Further, this solution is anomalous in that the above branch extends to the forbidden region $\Delta > 0$. The reason is that here the forcing (51) extends to infinity, unlike the δ-function forcing in (46), and the solution (52) has the same decay rate at infinity as the forcing. Hence the usual argument about why $\Delta < 0$ does not apply.

This suggests that (51) is not a good choice as a forcing term, and a better one is

$$K\,\mathrm{sech}^3(\gamma x). \tag{54}$$

Here, K is chosen so that the area under the forcing function is again unity. In this case again we seek a solution

$$A = a\,\mathrm{sech}(\gamma x). \tag{55}$$

Now the forcing (54) decays more rapidly at infinity than the solution (55). We find that

$$k_m \Delta = -\lambda \gamma^2 \quad \text{and} \quad a\left\{k_m \Delta + \frac{\nu a^2}{2}\right\} = \frac{K \omega_m \epsilon p_m}{2g^*}. \tag{56}$$

Note that (56) is in fact identical to (53) but now $\Delta < 0$ is required. But again the "dimpled" solutions are not found, and presumably again need numerical integration. Also, the expression (56) includes the branch with $a > 0$ which (53) does not allow.

6.3. Comparison of fNLS and nonlinear results

To make a connection with the nonlinear numerical results, in this section we choose the pressure distribution $U^2 p(x)/2$ to be the same as that used in the numerical results, but reduced for the present weakly nonlinear limit. That is, we let

$$p(x) = \exp\left[\frac{{x_b}^2}{x^2 - {x_b}^2}\right] \quad \text{for } |x| < x_b, \tag{57}$$

and zero elsewhere. As above the δ-function in (46) is then replaced by a smooth function such that the area under the curve of this function is unity. Thus we make the substitution

$$\delta(x) \to \frac{p(x)}{p_0} \quad \text{where } p_0 = \int_{-\infty}^{\infty} p(x)\,\mathrm{d}x.$$

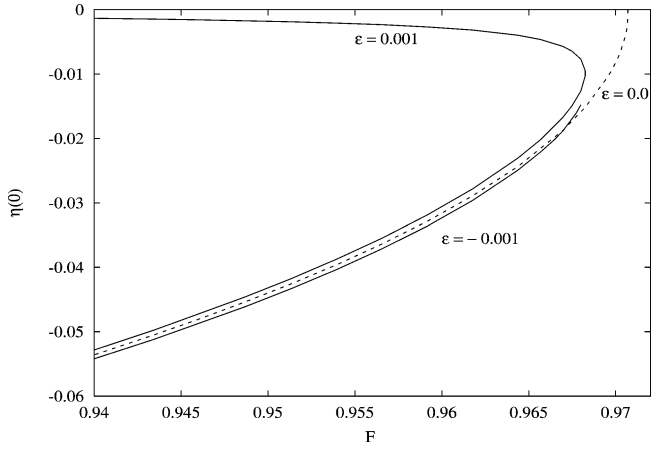

(a)

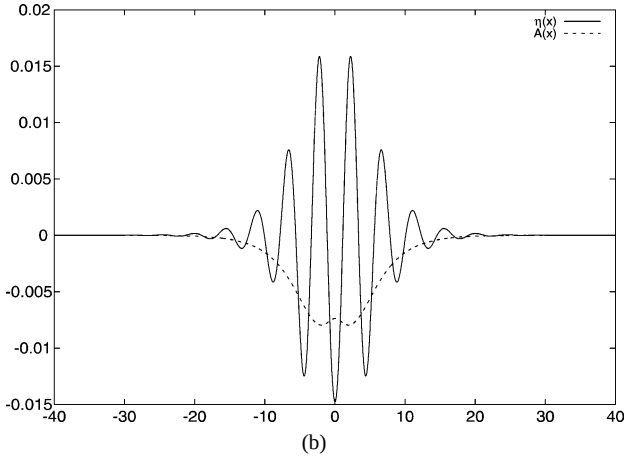

(b)

Fig. 11. (a) Relationship between F and $\eta(0)$ from fNLS results. (b) Free surface profile from the fNLS when $F = 0.968$ and $\epsilon = -0.001$.

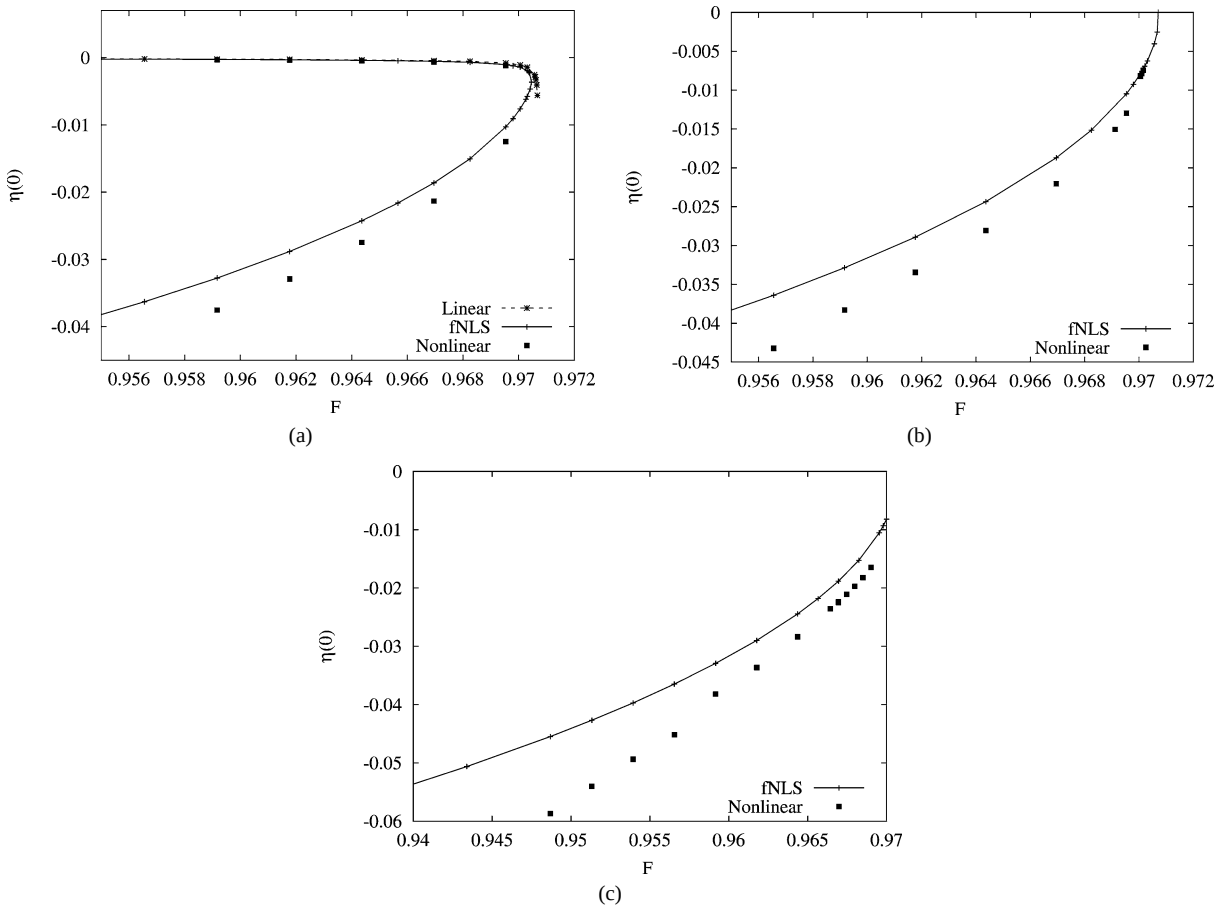

Fig. 12. Relationship between F and $\eta(0)$ in the case of depression waves when $\tau = 0.25$. (a) $\epsilon = 0.0001$; (b) $\epsilon = 0.0$; (c) $\epsilon = -0.0001$.

Then Eq. (46) becomes, in dimensionless coordinates based on length scale H and velocity scale $(gH)^{1/2}$,

$$(F - F_m)k_m A + \lambda_m A_{xx} + \nu_m |A|^2 A = \frac{F^2 \epsilon \omega_m p_m}{4p_0(1 + \tau k_m^2)} p(x). \tag{58}$$

Strictly speaking $F = F_m$ on the right-hand side, but we will retain F in the above equation. Here λ_m, ν_m are the non-dimensional values of λ, ν at $k = k_m$.

We will find $A(x)$ numerically by using a high-order Runge–Kutta method. To do this numerically, we set initial conditions at $x = L$ where $L \gg x_b$. That is, we put

$$A(x) = a_0 \exp(-2\gamma L), \qquad A_x = -2\gamma a_0 \exp(-2\gamma L),$$

where

$$\gamma^2 = -\frac{k_m(F - F_m)}{\lambda}.$$

We assume that A is real, and then integrate from L to 0. Then a_0 is varied until we can satisfy $\eta_x(x = 0) = 0$. Note that we need to find both elevation and depression waves, and presumably these have $a_0 > (<) 0$. Also, for this fNLS the change $\epsilon \to -\epsilon$ and $A \to -A$ leaves the equation unchanged. This implies that all solutions for $\epsilon < 0$ can be found as mirror images of those for $\epsilon > 0$. Thus, it is sufficient to solve for $\epsilon > 0$ and find both depression and elevation waves, since the branches for $\epsilon < 0$ are simply found by changing $A(0)$ to $-A(0)$ as above. Also since two branches have a turning point, there can be two solutions for a given F implying that for a fixed $\epsilon > 0$ (or < 0) there are potentially three solutions. Finally, the free surface profiles are obtained from (45),

$$\eta = 2A(x)\cos(k_m x).$$

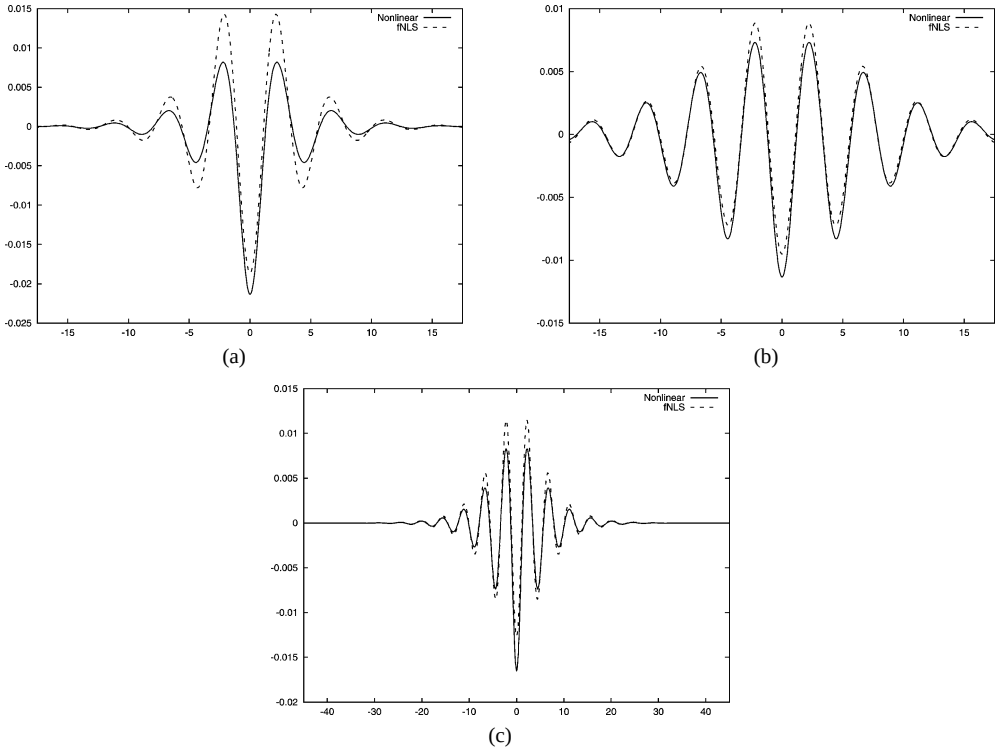

Fig. 13. Comparisons of free surface profiles for depression waves. (a) $F = 0.96695$, $\epsilon = 0.0001$; (b) $F = 0.96974$, $\epsilon = 0.0$; (c) $F = 0.96902$, $\epsilon = -0.0001$.

The values of ν and λ in the fNLS equation are scaled by using $\sqrt{gH}$ as a unit velocity and H as a unit length. When $\tau = 0.25$, the corresponding critical values are as follows: $k_m = 1.402$, $\omega_m = 1.361$, $F_m = 0.9707$, $\lambda_m = 0.045$, $\nu_m = 119.9$, $p_m = 0.4562$ and $p_0 = 0.6438$. Note that $\lambda_m \nu_m > 0$ for this value of τ as required. Indeed it can be shown that $\lambda_m \nu_m > 0$ for all $\tau, 0 < \tau < 1/3$.

6.3.1. Depression waves

For small ϵ, the fNLS model predicts the existence of all branches found numerically. The branches for $\epsilon = 0.001$, 0 and -0.001 for depression waves are shown in Fig. 11(a) (those for elevation waves are mirror images of these with the sign of ϵ reversed as discussed above). These branches correspond to the fully nonlinear results shown in Figs. 1 and 3. Interestingly while we see good qualitative agreement, the quantitative agreement is markedly better for depression waves than for elevation waves. Fig. 11(b) shows the free surface profile $\eta(x)$ and the envelope $A(x)$ obtained from integrating the fNLS equation (58). From Fig. 11(a) we see that the $\epsilon < 0$ branch crosses the unforced ($\epsilon = 0$) branch, and a "dimpled" solution exists above this unforced branch. This behavior agrees qualitatively with the analysis in Section 6.1 with the δ-forcing (compare also the results presented by Părău and Dias [10]). However, when we use the actual forcing, we see that the branch with negative forcing does exist, but lies below the unforced branch until the dimple appears, after which it lies above the unforced branch. In contrast, using the δ-function forcing places the "dimpled" branch always above the unforced branch, and in fact coincident with the "monotonic" branch.

Next we compare the depression wave solutions of the fNLS equation (58) with the numerical solutions of the fully nonlinear equations, and also with the linear solutions obtained from (9). For $\epsilon = 0.0001$, the relationship between $\eta(0)$ and F of the linear, fNLS and nonlinear solutions are shown in Fig. 12(a). As expected, the numerical solutions of (58) confirm the previous analysis corresponding to the bifurcation curve (56). Two solutions are found at the same value of F. That is, one solution (the upper curve) is the bifurcation from a uniform stream and the other (the lower curve) is the bifurcation from an envelope solitary wave. From Fig. 12(a), results from the fNLS model agree well with the fully nonlinear results along the upper curve and as F nears F_m. But unlike the fNLS solutions, the linear solutions for $\epsilon > 0$ are in good agreement with fNLS and nonlinear solutions only when F is not too close to F_m. Along the lower curve, we find that the differences in amplitude between the fNLS and nonlinear results emerge as F decreases away from F_m since the wave amplitude increases as F decreases. This behaviour

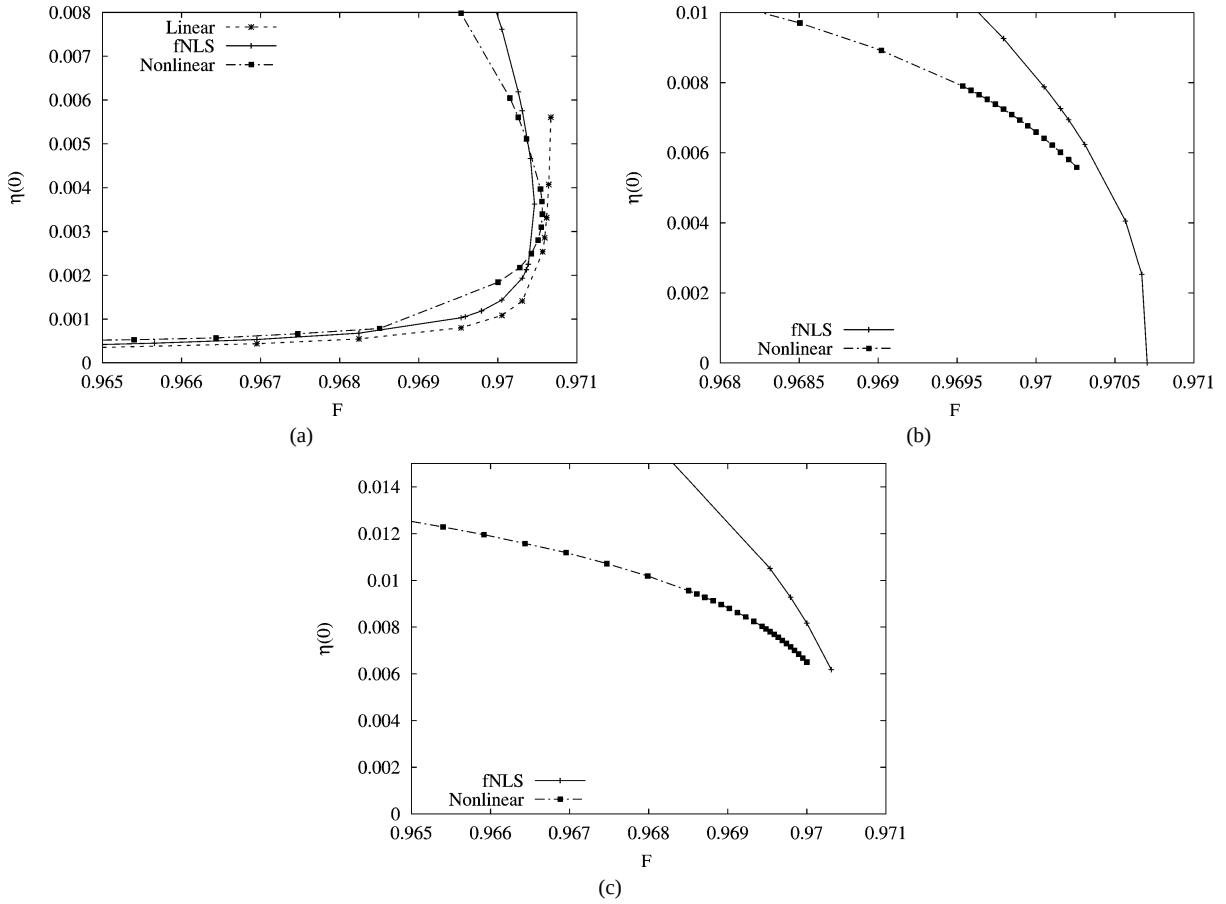

Fig. 14. Relationship between F and $\eta(0)$ in the case of elevation waves when $\tau = 0.25$. (a) $\epsilon = -0.0001$; (b) $\epsilon = 0.0$; (c) $\epsilon = 0.0001$.

of the fNLS solutions are consistent with the assumptions made in the derivation of the fNLS model. The comparison of the computed free surface profiles between fNLS and nonlinear results are shown in Fig. 13. The comparison for $\epsilon = 0.0001$ and on the lower branch is shown in Fig. 13(a). Although there is a difference in the amplitudes, the wavelength calculated from the two approaches is in good agreement with the predicted value $2\pi/k_m$.

A comparison of the depression solitary waves for $\epsilon = 0$ obtained from the NLS model and the fully nonlinear numerical solution are shown in Fig. 12(b), and a typical free surface profile is shown in Fig. 13(b). It is clear from these results that bifurcation occurs at the critical value F_m as expected (compare Buffoni, Champneys and Toland [22]), even although we are unable to obtain accurate nonlinear solutions as F approaches F_m due to inflexion points on the wave profile. Finally there also exist depression wave solutions in the case of $\epsilon < 0$, shown in Fig. 12(c) and Fig. 13(c). Again, results from fNLS and nonlinear problems are in good agreement when the wave amplitude is relatively small.

6.3.2. Elevation waves

For $\tau < 1/3$, we have found that elevation waves exist for both $\epsilon > 0$ and < 0 as predicted by the fNLS model. This is different from the case of $\tau > 1/3$ when solutions can only be found when $\epsilon < 0$ (MAG1). For $\epsilon < 0$ and $\tau < 1/3$, the branches of elevation waves from the linear theory, the fNLS model and the fully nonlinear results are shown in Fig. 14(a). There are two types of solutions, one (the lower curve) is a perturbation from a uniform stream, and the other (the upper curve) is a perturbation from an envelope solitary wave. The fNLS results agree well with the nonlinear results when the wave is of small amplitude and F is close to F_m, while linear results give better prediction to the perturbed solutions from the uniform stream. The corresponding comparison of the computed free surface profiles on the upper curve for $\epsilon = -0.0001$ is shown in Fig. 15(a).

It should be noted that fNLS is not a good model equation to described wave solutions when $|F - F_m|$ is sufficiently large. In that case the nonlinear solution is a better choice to gain insight into the solution behaviours. Figs. 14(b) and 15(b) give a comparison of elevation solitary waves ($\epsilon = 0$) obtained from the NLS model with the fully nonlinear results. These again show that elevation solitary wave solutions bifurcate from the critical value F_m, just as for depression waves. But we recall here that

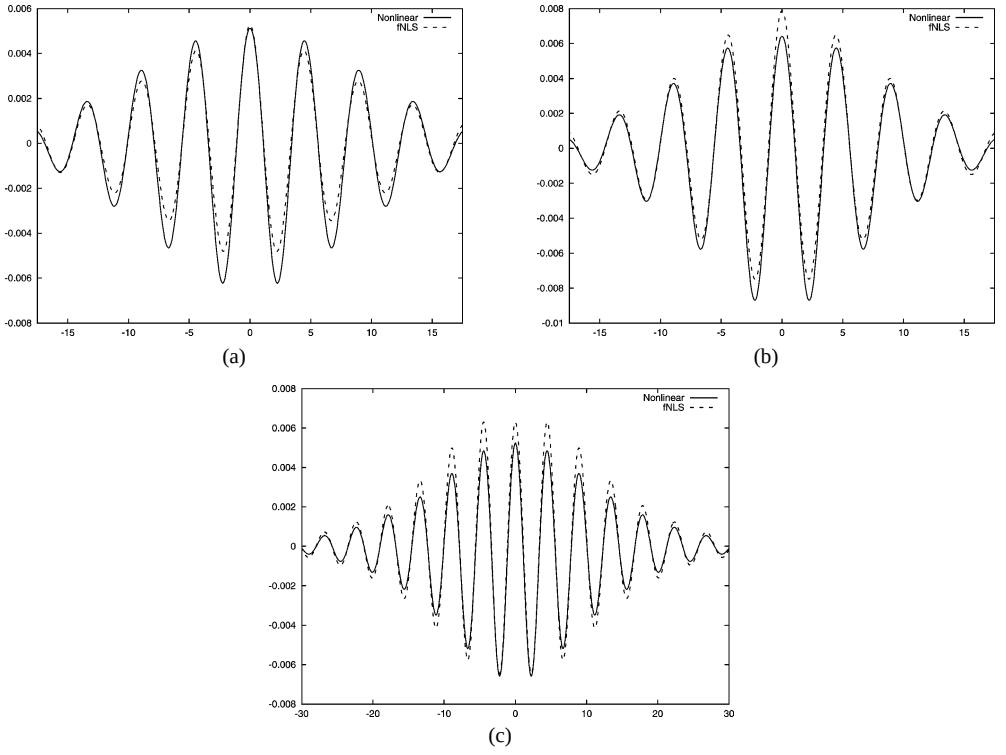

Fig. 15. Comparisons of free surface profiles for elevation waves. (a) $F = 0.97036$, $\epsilon = -0.0001$; (b) $F = 0.97005$, $\epsilon = 0.0$; (c) $F = 0.97026$, $\epsilon = 0.0001$.

the NLS and fNLS model predicts complete symmetry between depression and elevation waves. However, although this does occur in the limit as the wave amplitude decreases and $F \to F_m$ it is apparent from a comparison of Fig. 1 and Fig. 3 that this is not so for the fully nonlinear problem, where marked differences emerge as F decreases.

Finally in Figs. 14(c) and 15(c) we show the comparisons for elevation waves with $\epsilon > 0$. Note that the free surface profile obtained from the fNLS shown in Fig. 15(c) corresponds to a "dimpled" envelope solution of the fNLS equation with $A(x) > 0$. Again the qualitative agreement with the fNLS model is evident.

7. Discussion

In this paper we have presented some numerical results for the calculation of symmetric steady subcritical free surface flows due to an applied pressure distribution. Both gravity and surface tension effects are taken into account, and in this paper we have considered the case of gravity-dominated waves when the Bond number, $\tau < 1/3$, thus complementing the case $\tau > 1/3$ reported in our companion paper MAG1. Of course, except when τ is very close to zero, it has to be said that the results reported here for $\tau = 0.25$ have only limited application, since they apply for such shallow water depths that it is unrealistic to neglect dissipation, as we have done here. However, we feel that nevertheless it is useful to expand the known results for unforced solitary waves to a context of forced waves in this particular problem where numerical results for finite-amplitude waves can be obtained, in order to increase our understanding of nonlinear waves in general. Also, we expect these results to persist in qualitative form as τ is decreased, although the numerical calculations become extremely lengthy when τ is small.

Our numerical results show that both depression and elevation localized forced waves exist. It is found that depression and elevation waves exist for both positive ($\epsilon > 0$) and negative forcing ($\epsilon < 0$). The solution branches which plot wave amplitude versus the Froude number F is multivalued for depression waves when $\epsilon > 0$ and for elevation waves when $\epsilon < 0$. One solution is a perturbation from the uniform flow and the other is a perturbation of a solitary wave. We found only one branch, which is a perturbation of the solitary wave, for depression waves when $\epsilon < 0$ and for elevation waves when $\epsilon > 0$. In the case of depression waves, as F decreases, both these wave branches exhibit a limiting configuration with a trapped bubble.

To obtain insight into our numerical results, we considered both the linearized theory and a weakly nonlinear theory leading to the forced nonlinear Schrödinger (fNLS) equation. In the case of depression waves, for ϵ is small and positive, the bifurcation

diagram from the weakly nonlinear analysis of the fNLS model closely fits the numerical results, indicating that the forced solutions are bifurcations from an envelope solitary wave. On the upper part of this branch, the linearized theory can also predict the bifurcation from the uniform flow state, provided that F is not too close to F_m. The fNLS model can also predict the depression wave when $\epsilon = -0.0001 < 0$. Similar conclusions can be made for elevation waves as then the fNLS model predicts the same behaviour but for the opposite sign of ϵ. But in this case for the fully nonlinear results, while agreeing as expected as the wave amplitude decreases and $F \to F_m$, significant differences emerge as F decreases. Our numerical results show that as F decreases, the number of inflexion points on the free surface decrease, while the wave amplitude increases to a maximum value and then decreases again. The fNLS model cannot predict this behaviour.

Also, some wave solutions in the form of multi-hump solutions were obtained in our numerical calculations. We have reported here some typical behaviour as the flow parameters are varied. Further study is needed to understand these solutions and any connection with weakly nonlinear models.

Acknowledgements

The first author would like to thank the Department of Mathematical Sciences, Loughborough University for their kind support, and Prof. J.-M. Vanden-Broeck at the University of East Anglia for some useful comments. This research was financially supported by the Thailand Research Fund through the Royal Golden Jubilee PhD. Program (Grant No. PHD/0189/2542) to the first and last authors.

References

[1] Lord Rayleigh, The form of standing waves on the surface of running water, Proc. London Math. Soc. 15 (1883) 69.
[2] M. Maleewong, J. Asavanant, R. Grimshaw, Free surface flow under gravity and surface tension due to an applied pressure distribution I Bond number greater than one-third, Theoret. Comput. Fluid Dynamics, accepted for publication.
[3] T.R. Akylas, On the excitation of long nonlinear water waves by a moving pressure distribution, J. Fluid Mech. 141 (1993) 455–466.
[4] T.R. Akylas, Envelope solitons with stationary crests, Phys. Fluids A 5 (1993) 789–791.
[5] V.E. Zakharov, Stability of periodic waves of finite amplitude on the surface of a deep fluid, J. Appl. Mech. Tech. Phys. 2 (1968) 190–194.
[6] H. Hasimoto, H. Ono, Nonlinear modulation of gravity waves, J. Phys. Soc. Japan 33 (1972) 805–811.
[7] A. Davey, K. Stewartson, On three dimensional packets of surface waves, Proc. Roy. Soc. London Ser. A 338 (1974) 101–110.
[8] T. Kawahara, Nonlinear self-modulation of capillary-gravity waves on liquid layer, J. Phys. Soc. Japan 38 (1975) 265–270.
[9] V.D. Djordjevic, L.G. Redekopp, On two dimensional packets of capillary-gravity waves, J. Fluid Mech. 79 (1977) 703–714.
[10] E. Părău, F. Dias, Ondes solitaires forcées de capillarité-gravité, C. R. Acad. Sci. Paris, Ser. I 331 (2000) 655–660.
[11] D.C. Calvo, T.R. Akylas, Stability of steep gravity-capillary solitary waves in deep water, J. Fluid Mech. 452 (2002) 123–143.
[12] J.-M. Vanden-Broeck, F. Dias, Gravity-capillary solitary waves in water of infinite depth and related free surface flows, J. Fluid Mech. 240 (1992) 549–557.
[13] F. Dias, D. Menasce, J.-M. Vanden-Broeck, Numerical study of capillary-gravity solitary waves, Eur. J. Mech. B Fluids 15 (1996) 17–36.
[14] J.K. Hunter, J.-M. Vanden-Broeck, Solitary and periodic gravity-capillary waves of finite amplitude, J. Fluid Mech. 134 (1983) 205–219.
[15] R. Grimshaw, G. Iooss, Solitary waves of a coupled Korteweg–de Vries system, Math. Comput. Simulation 64 (2003) 31–40.
[16] C.J. Amick, K. Kirchgässner, A theory of solitary waves in the presence of surface tension, Arch. Rational Mech. Anal. 105 (1989) 1–49.
[17] G. Iooss, K. Kirchgässner, Bifurcation d'ondes solitaires en présence d'une faible tension superficielle, C. R. Acad. Sci. Paris, Ser. I 311 (1990) 265–268.
[18] F. Dias, G. Iooss, Water waves as a spatial dynamical system, in: Friedlander, Serre (Eds.), Handbook of Mathematical Fluid Dynamics, vol. 2, Elsevier, 2003, pp. 443–499.
[19] L.W. Schwartz, Nonlinear solutions for an applied over pressure on a moving stream, J. Engrg. Math. 12 (1981) 147–156.
[20] J. Asavanant, J.-M. Vanden-Broeck, Free surface flows past a surface piercing object of finite length, J. Fluid Mech. 273 (1994) 109–124.
[21] M.S. Longuet-Higgins, Limiting forms of capillary-gravity waves, J. Fluid Mech. 194 (1988) 351–375.
[22] B. Buffoni, A.R. Champneys, J.F. Toland, Bifurcation and coalescence of a plethora of homoclinic orbits for a Hamiltonian system, J. Dynam. Differential Equations 8 (1996) 221–279.